



## Using a multi-receiver survey of apparent electrical conductivity to reconstruct a Holocene tidal channel in a polder area

Timothy Saey<sup>a,\*</sup>, Mohammad Monirul Islam<sup>a</sup>, Philippe De Smedt<sup>a</sup>, Eef Meerschman<sup>a</sup>, Ellen Van De Vijver<sup>a</sup>, Alexander Lehouck<sup>b,c</sup>, Marc Van Meirvenne<sup>a</sup>

<sup>a</sup> Research Group Soil Spatial Inventory Techniques, Faculty of Bioscience Engineering, Ghent University, Coupure 653, 9000 Gent, Belgium

<sup>b</sup> Abdijmuseum Ten Duinen 1138, Koninklijke Prinslaan 6-8, 8670 Koksijde, Belgium

<sup>c</sup> Department of Medieval History, Faculty of Arts and Philosophy, Sint-Pietersnieuwstraat 35, 9000 Gent, Belgium

### ARTICLE INFO

#### Article history:

Received 31 August 2011

Received in revised form 26 January 2012

Accepted 5 February 2012

#### Keywords:

Proximal soil sensor

Eca

Electromagnetic induction

Tidal channel

Depth modelling

Three-layered soil model

### ABSTRACT

Most geological and soil maps are not detailed enough to represent the high lateral and vertical textural variability in the subsoil of coastal lowlands. Intensive sampling campaigns need to be carried out to quantify this variability. As an alternative, a proximal soil sensing procedure based on a single survey with an electromagnetic induction instrument was used to map a 6.5 ha Holocene tidal area in Belgium. We investigated the effectiveness of a multi-receiver apparent electrical conductivity (Eca) survey for mapping the trace of tidal paleochannels. From a limited number of augerings, a three-layered soil was observed composed of a clayey top layer, a clayey infilling of the tidal channel above a subsoil consisting of coarse sandy material. A fitting procedure allowed modelling the conductivities of both subsurface layers, after which the four simultaneous Eca measurements were combined to model the depth of the interfaces between the three layers. The predictions were validated by 16 depth observations along a 150 m transect. A correlation coefficient of 0.91, with an average error of 0.23 m, was found between the predicted and measured depths of the clay-sand interface. We concluded that the dense Eca measurements (2 by 2 m resolution) allowed reconstructing a precise three-dimensional representation of the tidal channels.

© 2012 Elsevier B.V. All rights reserved.

### 1. Introduction

After centuries of soil tillage, the topsoil has lost most traces of natural and anthropogenic events in most European countries. Although the subsoil might still contain useful information, it is less accessible. In the past soil augerings were the major modus to conduct such investigations. These are punctual observations, becoming very costly when a large number of data is required to characterize the small-scale spatial variability (Vitharana et al., 2008). Moreover, most soil maps aimed at supporting agricultural developments and thus focused on the topsoil (Kværnø et al., 2007). On the other hand, geological maps represent an overview of the geographical distribution of outcropping deposits, often at a rather coarse scale preventing detailed interferences (Smirnov et al., 2008).

Soil and geological maps are often of little use in the Holocene coastal plains because the sedimentary sequences are characterized by a high lateral and vertical variability (Bertrand and Baeteman, 2005). Yet, they still contain information about the recent history of these landscapes, which, in Europe, were cultivated in medieval times. Questions about the landscape build-up at that time and human

interferences for land reclamation are open to modern historians, geomorphologists and archaeologists.

The recent introduction of non-invasive proximal soil sensing systems offers new perspectives to study subsoil variability in detail providing several advantages over traditional invasive measurement methods (Cockx et al., 2007; Saey et al., 2008, 2009b). These advantages include lower cost, increased efficiency and above all, much denser results (Sudduth et al., 2005). Generally, these systems aim at mapping differences in electrical conductivity that could be linked to variations in water content and/or conductivity of the pore water and/or soil texture within the unsaturated zone, both laterally and vertically (Massuel et al., 2011). A promising technique is electromagnetic induction (EMI) (Brenning et al., 2008). With EMI, bulk measurements of the soil apparent electrical conductivity (Eca) can be obtained, which act as an indicator of important soil properties such as clay content, moisture content, and organic matter content (Domsch and Giebel, 2004; McBratney et al., 2005; Saey et al., 2009b; Sudduth et al., 2001). Additionally to the fact that geospatial Eca measurements are reliable, quick, and easy to obtain, they can be made mobile, allowing to cover larger areas fairly efficiently (Corwin et al., 2006).

The objective of this research was to develop a methodology to predict the interfaces between contrasting layers in a three-layered soil, or more specifically to map the upper and lower interface of a

\* Corresponding author. Tel.: +32 9 264 60 42; fax: +32 9 264 62 47.  
E-mail address: [Timothy.Saey@UGent.be](mailto:Timothy.Saey@UGent.be) (T. Saey).

Holocene tidal channel in a coastal area. A fitting procedure must allow to simplify the three-layered soil conductivity model, to be able to integrate the multiple ECa measurements of the multi-receiver EMI sensor. This way, the potential to simultaneously model two ‘sharp’ interface depths across the field should be evaluated. Quantifying the dimensions of the tidal channel, as specific objective, should resolve questions about the medieval landscape in the coastal plain.

## 2. Study area

The study area is a 6.5 ha agricultural field located in the western part of the coastal plain of Belgium (central coordinates: 51°06′48″N and 2°42′04″E) (Fig. 1). The coastal plain is part of the lowlands of the southern North Sea which stretch from Cap Blanc Nez in northern France to Skagen in Denmark. The Belgian coastal plain is a polder area of about 15–20 km wide with an extension in the western part of the plain along the river IJzer. The plain was created by embankment following post-glacial sea-level rise and is situated behind a belt of aeolian sand dunes (Baeteman, 1999; 2008; Baeteman and Declercq, 2002). Its particular microrelief results from both natural and man-induced processes. Sea-level rise at the onset of the Holocene initiated peat formation and sediment accumulation behind the coastal barrier. A decrease in sea-level rise starting around 7500 year BP caused increasing sedimentation in the newly formed tidal basin. As sea-level rise continued to drop ca. 5500–5000 year BP, the thickest peat layers accumulated, lasting until about 1500 year BP (Baeteman, 1991; 2008). Throughout the evolution of the coastal plain, tidal channels were formed in the peat layers and the underlying sediments, which in their turn were filled up by sandy and, in more recent systems, clayey sediments. Radiocarbon dating showed that these tidal channels were active until the 7th century AD (Ervynck et al., 1999).

In the larger study area, which has been part of the IJzer Estuary and palaeovalley, late-Holocene sand and silt deposits are dominating. Sand-filled tidal channels were formed during the *La Tène* (from 560 year BC) and Roman period, incising through the older deposits and causing peat erosion. Finally, the channels were filled with clayey sediments under calm and smooth conditions, which started in the 7th century AD (Baeteman, 2008). Unprocessed data of the recent archaeological and pedological research will inform us about the exact end date of the infill. The soil characteristics are rather uniform throughout the entire study site. The topsoil (plough layer and the bioturbated zone beneath) consists of clayey sediments overlaying the sandy deposits. The present topography of our study area (Fig. 1) is

flat, and the topsoil has been homogenised by tillage. The national soil map (1/20,000) is not very detailed, it shows two dominant soil series within our study site, both indicating heavy clay and clay of varying thickness overlying sandy material.

## 3. Multi-receiver electromagnetic induction (EMI) sensor

In its simplest configuration, a proximal EMI soil sensor consists of two coils separated by a given fixed distance. A primary magnetic field ( $H_p$ ) is created by the transmitting coil. This field creates eddy currents in the soil below, which induce their own magnetic field ( $H_i$ ). The induced secondary field is superimposed on the primary field and both  $H_p$  and  $H_i$  are measured by the receiving coil (McNeill, 1980). From this response the ECa of the bulk soil can be obtained. We used the DUALEM-21S instrument (DUALEM, Milton, Canada) which consists of one transmitter coil and four receiver coils located at spacings of 1, 1.1, 2 and 2.1 m (Saey et al., 2009a). The 1 and 2 m transmitter-receiver pairs form a vertical dipole mode (1V and 2V), while the 1.1 and 2.1 m pairs form a perpendicular dipole mode (1P and 2P). Both transmitter-receiver spacing and orientation determine the depth and weighting response pattern of the signal. The cumulative response (expressed as % of the measured signal, relative to 1) from the soil volume above a depth  $z$  (in m) was given by McNeill (1980) for the vertical ( $R_v(z)$ ) dipole mode and by Wait (1962) for the perpendicular ( $R_p(z)$ ) dipole mode:

$$R_v(z) = 1 - \left( 4 \frac{z^2}{s^2} + 1 \right)^{-0.5} \quad (1)$$

$$R_p(z) = 2 \frac{z^2}{s^2} \left( 4 \frac{z^2}{s^2} + 1 \right)^{-0.5} \quad (2)$$

with  $s$  being the transmitter-receiver spacing.

These cumulative response functions allow the determination of the depth of exploration (DOE), defined as the depth where 70% of the response is obtained from the soil volume above this depth down from the soil surface. This DOE differs for the different coil configurations: 0.5 m, 1.0 m, 1.5 m and 3.2 m for the 1P, 2P, 1V and 2V coil configurations respectively (Saey et al., 2009a). Measurements of soil temperature allowed the conversion of the measurements to a reference temperature (conventionally 25°C is used).

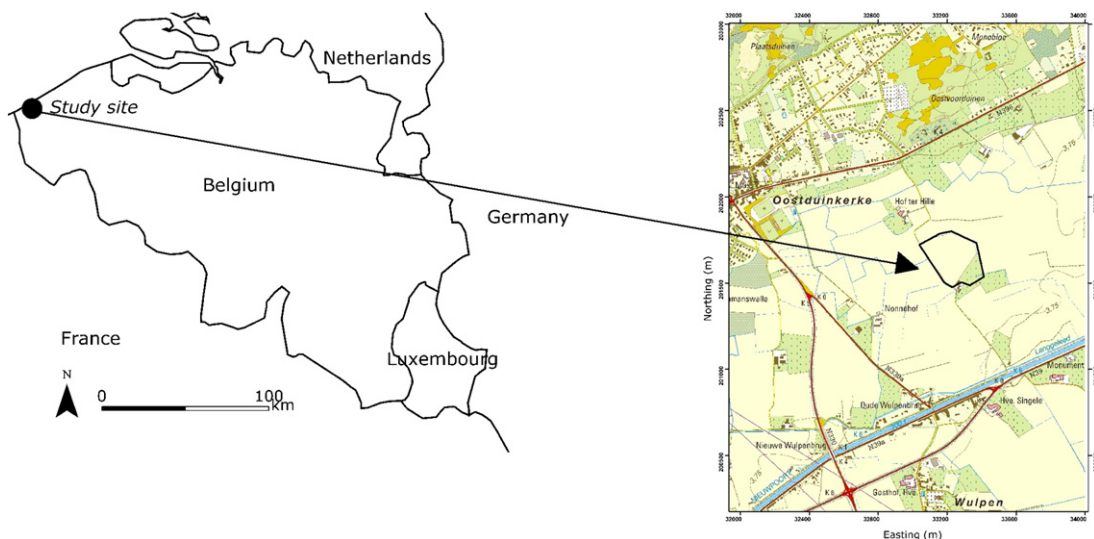


Fig. 1. Localisation of the study site in Belgium and topographic map with indication of the study site (black).

#### 4. ECa survey

The ECa of the study site was investigated with the DUALEM-21S proximal EMI soil sensor. Therefore the sensor was put in a non-metal sled and pulled behind an all-terrain vehicle at a speed of about 6–10 km h<sup>-1</sup>, crossing the field at parallel lines 1.7 m apart. The four simultaneous ECa measurements were recorded by a field computer. The computer was connected to a Trimble AgGPS332, allowing to georeference the ECa measurements with a pass-to-pass accuracy of approximately 0.10 m. Within lines, measurement intervals were at about 1 m. This yielded a measurement density of approximately 1 observation per 2 m<sup>2</sup>.

Table 1 shows the summary statistics of the 4 × 39 326 ECa measurements taken with the DUALEM-21S sensor. The mean and maximum values of the ECa<sub>p,2</sub> and ECa<sub>v,2</sub> are almost identical, and larger than the shallower ECa<sub>p,1</sub> and the deeper ECa<sub>v,2</sub>, indicating that on average the topsoil and deeper material are less conductive, probably caused by a lower clay content compared to the soil volume between 0.5 m and 1.5 m (Saey et al., 2009b). The negative minimum value of the ECa<sub>p,1</sub> (−28 mS m<sup>-1</sup>) and ECa<sub>p,2</sub> (−36 mS m<sup>-1</sup>) and same very high maximum values (267 mS m<sup>-1</sup>) of the ECa<sub>p,1</sub> are caused by anomalies (like small pieces of metal) in the topsoil (Saey et al., 2011). The standard deviations are similar for the four ECa measurements.

Ordinary kriging was chosen to interpolate the sensor data to a regular 0.5 m by 0.5 m grid (Triantafyllis et al., 2001; Wilson et al., 2005). This geostatistical technique ensures unbiased estimates with minimal estimation variance. Moreover, kriging includes declustering the sensor data, which accounts for the denser within-line measurements (1.0 m). Ordinary kriging weights are derived from a variogram, which is a model of the spatial structure (Goovaerts, 1997; Webster and Oliver, 2007). We modeled the variograms by manually fitting a variogram model to the data. A maximum of 64 neighbours was used within a circular search area around the location being interpolated. The variogram parameters are shown in Table 2.

Fig. 2 shows the interpolated ECa maps of the study area. The patterns are analogue for the four simultaneous measurements, but the absolute values differ. A clear fluvial structure is visible on all maps, although no trace of it is observable at the surface (the topography is flat). This creek pattern is less clear on the ECa<sub>p,1</sub>, indicating that this tidal channel is situated below the topsoil. This creek was most likely a tidal channel, connected to the North Sea. Additional linear features cross the field, which indicate more recent human activities (like drainpipes or buried ditches).

#### 5. Punctual EC-measurements and depth observations

The standard EC-probe set for soil conductivity measurements consists of an EC-probe and an earth resistivity meter (Eijkkelkamp Agrisearch Equipment, Giesbeek, The Netherlands). Measurement of the soil resistivity using four electrodes is based on the Wenner-method, applied by Rhoades and Van Schilfgaarde (1976) for the development of an EC-probe. It allows to measure directly in situ the electrical resistivity (which is the inverse of EC) of a limited (elliptic)

**Table 1**  
Descriptive statistics (*m*: mean, *min*: minimum, *max*: maximum, *s*: standard deviation) of ECa<sub>p,1</sub>, ECa<sub>p,2</sub>, ECa<sub>v,1</sub> and ECa<sub>v,2</sub> for the study site (39326 measurement points).

Variable	<i>m</i> (mS m <sup>-1</sup> )	Min (mS m <sup>-1</sup> )	Max (mS m <sup>-1</sup> )	<i>s</i> (mS m <sup>-1</sup> )
ECa <sub>p,1</sub>	46	−28	267	7
ECa <sub>p,2</sub>	57	−36	130	9
ECa <sub>v,1</sub>	58	23	140	9
ECa <sub>v,2</sub>	54	11	96	10

**Table 2**

Variogram model parameters for the 4 simultaneous ECa measurements with the DUALEM-21S, the soil surface elevation (*Z*) and the modeled depth of the topsoil (*z*<sub>1</sub><sup>\*</sup>) and interface (*z*<sub>2</sub><sup>\*</sup>).

Variable	Model	Nugget	Slope	Sill	Range (m)
ECa <sub>p,1</sub>	Spherical	7	−	12	20
	Linear	7	0.95	−	−
ECa <sub>p,2</sub>	Linear	4	2.65	−	−
ECa <sub>v,1</sub>	Linear	0	2.25	−	−
ECa <sub>v,2</sub>	Gaussian	0.5	−	20	20
	Linear	0.5	1.4	−	−
<i>Z</i>	Spherical	0.055	−	0.067	20
<i>z</i> <sub>1</sub> <sup>*</sup>	Gaussian	0	−	0.001	20
<i>z</i> <sub>2</sub> <sup>*</sup>	Gaussian	0.025	−	0.1	20

soil volume of 80 cm<sup>3</sup> of soil around the probe down to a depth of 1 m. A temperature sensor is also present to convert the measurements to the reference temperature of 25 °C.

To calibrate the sensor measurements, we selected 20 locations according to a 50 by 50 m grid scheme across the field (Fig. 2(b)). Using the EC-probe, 20 measurements of the topsoil 0–0.3 m (EC<sub>1</sub>) were obtained. The average (*m*) is 55 mS m<sup>-1</sup> with a standard deviation (*s*) of 12 mS m<sup>-1</sup>. At these 20 locations, the soil constitution was investigated by a hand auger. At each of these locations, the average thickness of the plough layer (*z*<sub>1</sub>) was 0.25 m with a small *s* of 0.06 m and the depth of the interface between the marine clay and the underlying coarse sand (*z*<sub>2</sub>) was on average 1.55 m with a high *s* of 0.69 m. This depth-interface was clearly observable.

Moreover, we positioned a 150 m long transect “AB” in such a way that both high and low ECa values were visited (Fig. 2(a)). Along this 150 m long transect, 16 observations were made by a hand auger at regular intervals.

Fig. 3 shows the results of the auger observations as a cross section of the soil constitution. In general, the sand (layer 3) was found at a depth of 1 to 1.2 m. However, when we reached the tidal channel, this interface (*z*<sub>2</sub>) dropped to a depth of about 2.6–2.8 m (from about 105 m from the start of the transect). It will be clear that subsoil variability will have consequences in terms of agricultural land use (nutrient availability and leaching, etc.), but also for other land activities such as building construction.

#### 6. Depth modelling

The four simultaneous ECa measurements were used to model the EC's of the underlying layers (EC<sub>2</sub> and EC<sub>3</sub>) and *z*<sub>2</sub><sup>\*</sup>. In a three-layered soil build-up where coarse sand (layer 3) is situated below marine clay (layer 2) and a topsoil (layer 1; measured thickness 0.3 m (= *z*<sub>1</sub>)), the measured ECa can be estimated by summing the conductivities and depth-weighted contributions of each layer. The conductivity of the topsoil (EC<sub>1</sub>) was taken as the mean of the EC-borehole measurements. For every *z*<sub>2</sub>, the corresponding ECa<sub>p,s</sub> and ECa<sub>v,s</sub> can be expressed as a function of the apparent conductivity values of the three layers (EC<sub>1</sub>, EC<sub>2</sub> and EC<sub>3</sub>) respectively:

$$ECa_{v,s} = [R_{v,s}(z_1) - R_{v,s}(z_s)] \cdot EC_1 + [R_{v,s}(z_2^*) - R_{v,s}(z_1)] \cdot EC_2 + [1 - R_{v,s}(z_2^*)] \cdot EC_3 \quad (3)$$

$$ECa_{p,s} = [R_{p,s}(z_1) - R_{p,s}(z_s)] \cdot EC_1 + [R_{p,s}(z_2^*) - R_{p,s}(z_1)] \cdot EC_2 + [1 - R_{p,s}(z_2^*)] \cdot EC_3 \quad (4)$$

with *z*<sub>s</sub> the height of the sensor above the soil. *R*<sub>p,s</sub>(*z*) and *R*<sub>v,s</sub>(*z*) are the cumulative response function of the perpendicular and vertical

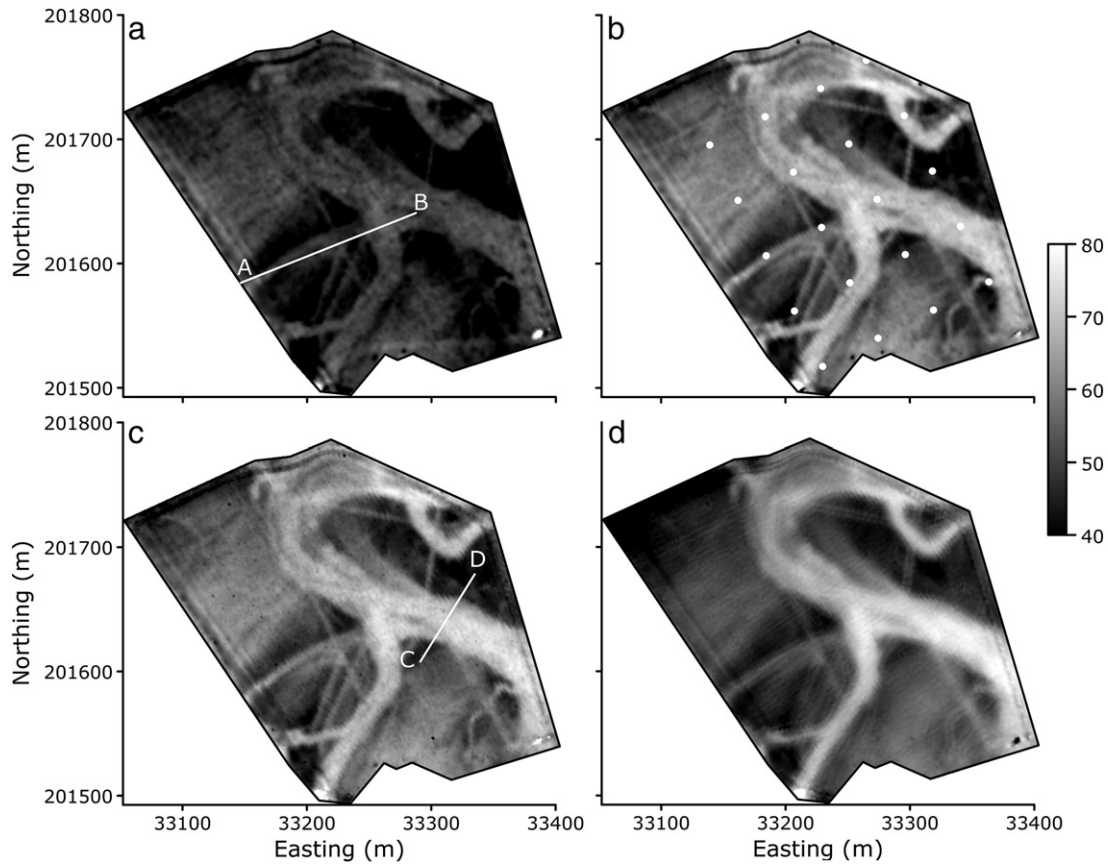


**Fig. 2.** Interpolated apparent electrical conductivity (ECA) map in the 1P coil configuration with localization of transect AB (a), in the 2P coil configuration with 20 points in a 50 by 50 m grid (b), in the 1 V with localisation of transect CD (c) and in the 2 V coil configuration (d) (all in  $\text{mS m}^{-1}$ ).

coil configuration with intercoil spacing  $s$  (Eqs. (1) and (2)) above a depth  $z$ . The cumulative responses from the top ( $\text{EC}_1$ ), clay ( $\text{EC}_2$ ) and sand ( $\text{EC}_3$ ) layers are  $(R_{p,s}(z_1) - R_{p,s}(z_s))$ ,  $(R_{p,s}(z_2) - R_{p,s}(z_1))$  and  $(1 - R_{p,s}(z_2))$  for the perpendicular coil configurations and  $(R_{v,s}(z_1) - R_{v,s}(z_s))$ ,  $(R_{v,s}(z_2) - R_{v,s}(z_1))$  and  $(1 - R_{v,s}(z_2))$  for the vertical coil configurations.

The unknown and fixed parameters  $\text{ECa}_2$  and  $\text{ECa}_3$  will be empirically determined by fitting simultaneously the cumulative response function  $R_{p,s}(z_2)$  to the  $z_2 - \text{ECA}_{p,s}$  and  $R_{v,s}(z_2)$  to the  $z_2 - \text{ECA}_{v,s}$  observations. The procedure developed to fit simultaneously  $R_{p,s}(z_2)$  to the  $z_2 - \text{ECA}_{p,s}$  measurements and  $R_{v,s}(z_2)$  to the  $z_2 - \text{ECA}_{v,s}$  measurements is described here.

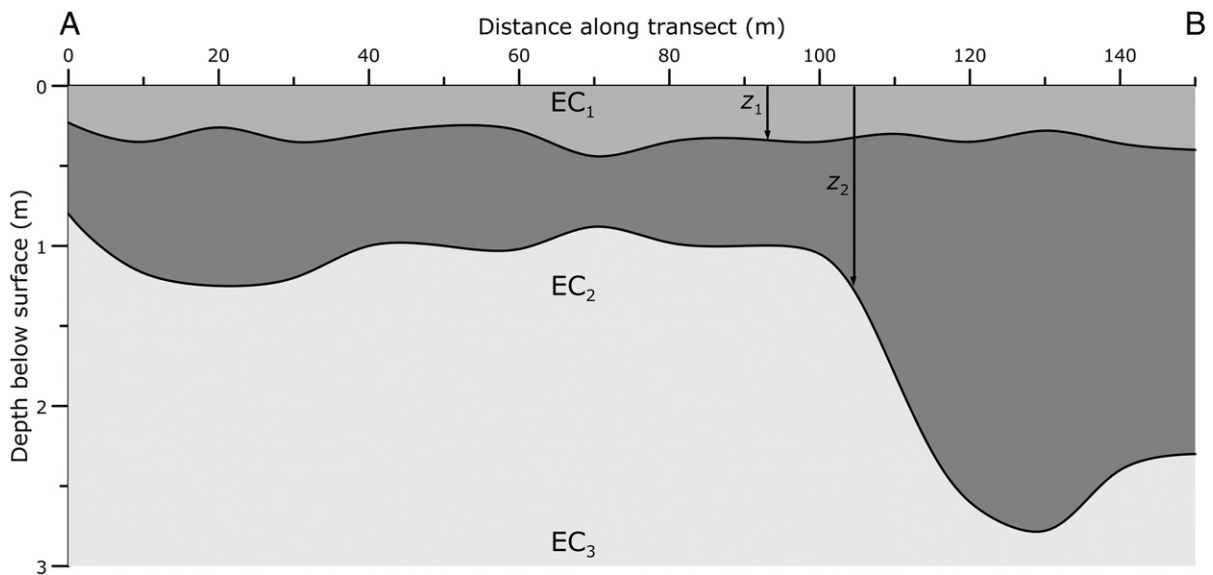


**Fig. 3.** Build-up of the soil along transect ABC, with indication of the conductivity of the three layers ( $\text{EC}_1$ ,  $\text{EC}_2$  and  $\text{EC}_3$ ) and the depth of the interfaces  $z_1$  and  $z_2$ .

Based on Eqs. (3) and (4),  $z_{2,p,s}^*$  and  $z_{2,v,s}^*$  can be modelled given the  $ECa_{p,s}$  and  $ECa_{v,s}$  measurements. Therefore,  $R_{p,s}(z_{2,p,s}^*)$  and  $R_{v,s}(z_{2,v,s}^*)$  were calculated given the  $ECa$  measurements and the conductivities of the three layers ( $EC_1$ ,  $EC_2$  and  $EC_3$ ):

$$R_{p,s}(z_{2,p,s}^*) = \frac{ECa_{p,s} - [R_{p,s}(z_1) - R_{p,s}(0.16)] \cdot EC_1 + R_{p,s}(z_1) \cdot EC_2 - EC_3}{EC_2 - EC_3} \quad (5)$$

$$R_{v,s}(z_{2,v,s}^*) = \frac{ECa_{v,s} - [R_{v,s}(z_1) - R_{v,s}(0.16)] \cdot EC_1 + R_{v,s}(z_1) \cdot EC_2 - EC_3}{EC_2 - EC_3} \quad (6)$$

These calculated  $R_{p,s}(z_{2,p,s}^*)$  and  $R_{v,s}(z_{2,v,s}^*)$  can be put into Eqs. (1) and (2) to obtain the modelled  $z_{2,p,s}^*$  and  $z_{2,v,s}^*$ :

$$z_{2,p,s}^* = \frac{s \cdot R_{p,s}(z_{2,p,s}^*)}{2 \cdot (1 - R_{p,s}(z_{2,p,s}^*))^{0.5}} - 0.16 \quad (7)$$

$$z_{2,v,s}^* = s \cdot \left( \frac{1}{4 \cdot [1 - R_{v,s}(z_{2,v,s}^*)]^2} - 0.25 \right)^{0.5} - 0.16 \quad (8)$$

To fit a cumulative depth response function to the  $z_2 - ECa_{p,s}$  and  $z_2 - ECa_{v,s}$  data points, the sum of the squared differences between  $z_2$  and  $z_{2,p,s}^*$  and between  $z_2$  and  $z_{2,v,s}^*$  were simultaneously minimized, thus for both perpendicular (1P and 2P) and vertical coil configurations (1V and 2V):

$$\sum_{i=1}^n [z_2(i) - z_2^*(i)]^2 = \min \quad (9)$$

with  $i$  the number of the observation and  $n$  the total amount of observations.

The parameters  $EC_2$  and  $EC_3$  were iteratively adjusted to obtain the smallest sum of the squared differences between  $z_2$  and  $z_2^*$  for both perpendicular and vertical coil configurations. This was done at the 20 locations where observations of  $EC_1$ ,  $z_1$  and  $z_2$  were performed. The resulting parameters  $EC_2$  and  $EC_3$  were found to be  $109 \text{ mS m}^{-1}$  and  $9 \text{ mS m}^{-1}$ . They were assumed to be uniform across the study site.

To evaluate the fitting approach, we compared the modelled  $ECa_{p,s}^*$  and  $ECa_{v,s}^*$  with the observed  $ECa_{p,s}$  and  $ECa_{v,s}$  at the 20 calibration locations. The modelled  $ECa_{p,s}^*$  and  $ECa_{v,s}^*$  were calculated with Eqs. (3) and (4) given the fitting parameters  $EC_2$  and  $EC_3$  ( $109 \text{ mS m}^{-1}$  and  $9 \text{ mS m}^{-1}$ ) and the observed  $z_2$  and  $EC_1$  at the 20 locations. Fig. 4 and Table 3 show that mainly  $ECa_{p,2}^*$  and  $ECa_{v,1}^*$  were well fitted ( $r$  approximately 0.8 and low MEE and RMSEE).  $ECa_{p,1}^*$  and  $ECa_{v,2}^*$  seemed to correspond less with the observed  $ECa$ 's, because the fitting parameters are the best compromise for all four coil configurations. Therefore, they are not optimal for each coil configuration separately.

The developed fitting procedure results in the two unknown parameters  $EC_2$  and  $EC_3$  ( $109 \text{ mS m}^{-1}$  and  $9 \text{ mS m}^{-1}$ ), which were assumed to be constant across the study site. Given these fixed parameters, a three-layered model can be established to model the unknown  $EC_1^*$ ,  $z_1^*$  and  $z_2^*$ , at each  $ECa$  measurement location, because these parameters were supposed to be variable across the study site. Due to the characteristic depth response profiles for each coil configuration, the following equations could be formulated, taking the height of the sensor above the soil surface into account (0.16 m):

$$\begin{aligned} ECa_{p,s} = & [R_{p,s}(z_1^* + 0.16) - R_{p,s}(0.16)] \cdot EC_1^* \\ & + [R_{p,s}(z_2^* + 0.16) - R_{p,s}(z_1^* + 0.16)] \cdot EC_2 \\ & + [1 - R_{p,s}(z_2^* + 0.16)] \cdot EC_3 \end{aligned} \quad (10)$$

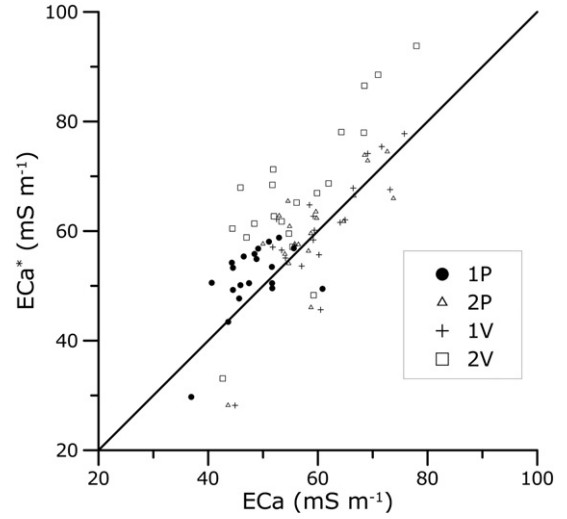


Fig. 4. Scatterplot of the predicted apparent electrical conductivity ( $ECa^*$ ) vs. the observed apparent electrical conductivity ( $ECa$ ) for the 1P, 2P, 1V and 2V coil configurations.

$$\begin{aligned} ECa_{v,s} = & [R_{v,s}(z_1^* + 0.16) - R_{v,s}(0.16)] \cdot EC_1^* \\ & + [R_{v,s}(z_2^* + 0.16) - R_{v,s}(z_1^* + 0.16)] \cdot EC_2 \\ & + [1 - R_{v,s}(z_2^* + 0.16)] \cdot EC_3 \end{aligned} \quad (11)$$

At each of the 39 326 measurement locations, the nonlinear Eqs. (10) and (11) for both 1 and 2 m coil configurations were combined to model the unknown parameters  $EC_1^*$ ,  $z_1^*$  and  $z_2^*$ . This system was solved with Matlab using the Levenberg–Marquardt algorithm (Marquardt, 1963).

## 7. Verification

The accuracy of the proposed model to predict  $z_2^*$  was evaluated by investigating the observed interface depths at 16 locations along the 150 m transect AB. At these locations, the observed depths were compared with the modelled depths (Fig. 5). The MEE and RMSEE were respectively 0.10 m and 0.23 m, which were acceptable for our purpose. The Pearson correlation coefficient  $r$  between  $z_2$  and  $z_2^*$  was 0.91, which was highly significant at  $\alpha = 0.05$ .

## 8. Reconstruction of the tidal channel

The elevation of the soil surface ( $Z$ ) was also available from our GPS measurements, with an absolute vertical accuracy in the order of 0.2–0.3 m. However, the relative point-by-point accuracy was much better, allowing the data to construct a surface of  $Z$ . It was interpolated with ordinary kriging and the result is given in Fig. 6(a).  $z_1^*$  and  $z_2^*$  were also interpolated using ordinary kriging under similar

Table 3

Pearson correlation coefficient ( $r$ ), MEE and RMSEE of the predicted apparent electrical conductivity ( $ECa^*$ ) vs. the observed apparent electrical conductivity ( $ECa$ ) for the 1P, 2P, 1V and 2V coil configurations.

	$r$	MEE ( $\text{mS m}^{-1}$ )	RMSEE ( $\text{mS m}^{-1}$ )
1P	0.55	3	6
2P	0.76	1	6
1V	0.80	0	6
2V	0.79	10	13

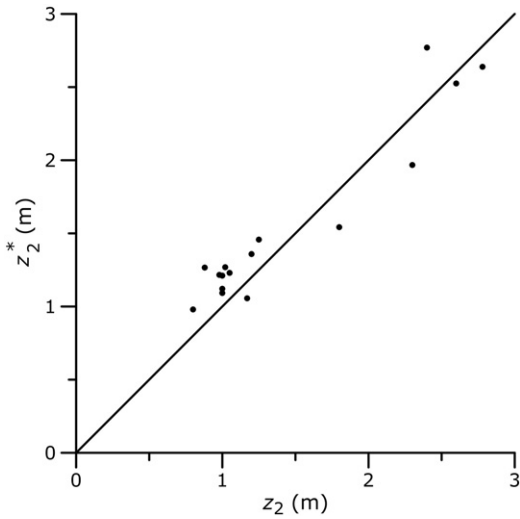


Fig. 5. Scatterplot of the predicted interface depth ( $z_2^*$ ) vs. the observed depth ( $z_2$ ).

conditions as the ECa maps. The variogram parameters are given in Table 2. Finally,  $z_1^*$  and  $z_2^*$  were subtracted from  $Z$  and the resulting maps are shown in Fig. 6(b) and (d), representing the elevation of both the topsoil-marine clay interface and the marine clay-coarse sand interface respectively. Fig. 6(c) shows the difference between  $z_1^*$  and  $z_2^*$  which mainly represents the channel pattern and its dimensions. Along 85 m transect CD (Fig. 6(b)) the tidal channel has a width of 44 m with a thickness of maximally 1.4 m. Its cross-section is approximately 46 m<sup>2</sup>, which means that with a hypothetical but reasonable water velocity of 1 m s<sup>-1</sup>, a flux of 46 000 l s<sup>-1</sup> could have flown through it (Fig. 7). The flow direction was to the south-

east and not to the north-west as was first expected from the proximity of the sea. So this channel must have been a tributary to a larger system.

It will be clear that such a tidal channel able of passing such large volumes of sea water in the area represented a potential threat for flooding and had to be diked-in before the area could be developed into cultivated land in historical times. During Roman times, or even before, it is likely that smaller ships could navigate on it towards or from the sea. In medieval times a parallel dike was constructed to the west of the channel protecting the hinterland against flooding, probably because the waterway was too big to be blocked itself. The dike however had to cross the westward oriented tributary and therefore a turn was made so to cut this waterway in a perpendicular way (see Fig. 6(d)). This finding opens new insights into the earliest development of the area. Therefore, tracking and modelling the further course of this channel is advisable.

9. Discussion

EMI and electrical resistivity tomography (ERT) are effective geophysical techniques for fast and high-resolution determination of the interface depths between contrasting soil layers at the field scale. As significant technological improvements have increased its spatial resolution, ERT is used to map the interface depths when there are highly contrasting resistivity levels between the soil layers (Coulouma et al., 2012). However, this technique encounters some limitations. A good contact between the soil and the electrodes is required, which can cause problems in dry and rocky soils (Samouëlian et al., 2005). Only recently, mobile systems were developed that allow identifying soil horizon thicknesses in three-dimensions (Lück and Rühlmann, 2008). Despite the fact that inverting the ERT-data is very time-consuming, it can only provide an approximative guide to the true geometry of the interface depths (Samouëlian et al., 2005).

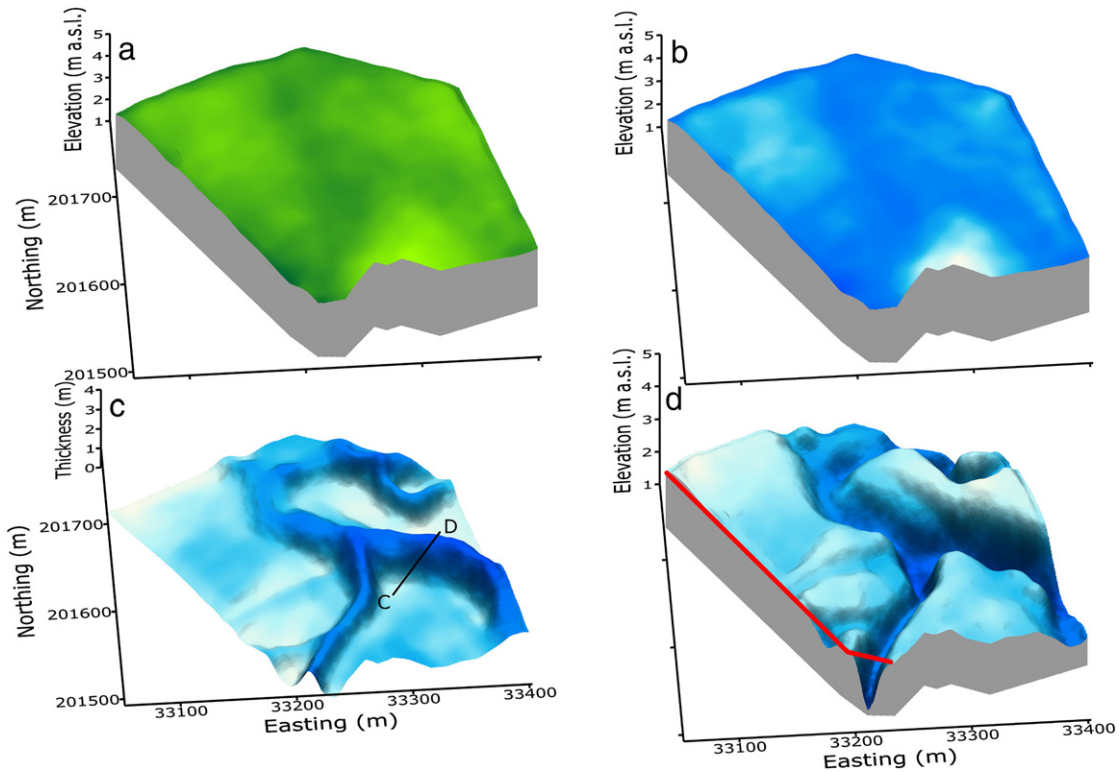


Fig. 6. The elevation of the current surface  $Z$  (a), the elevation of the topsoil-marine clay interface  $Z-z_1^*$  (b), the thickness of the marine clay  $z_2^*-z_1^*$  which mainly represents the pattern of the tidal channel with localization of transect CD (c) and the elevation of the marine clay-coarse sand interface  $Z-z_2^*$  with indication of the sea-dike (red) (d).

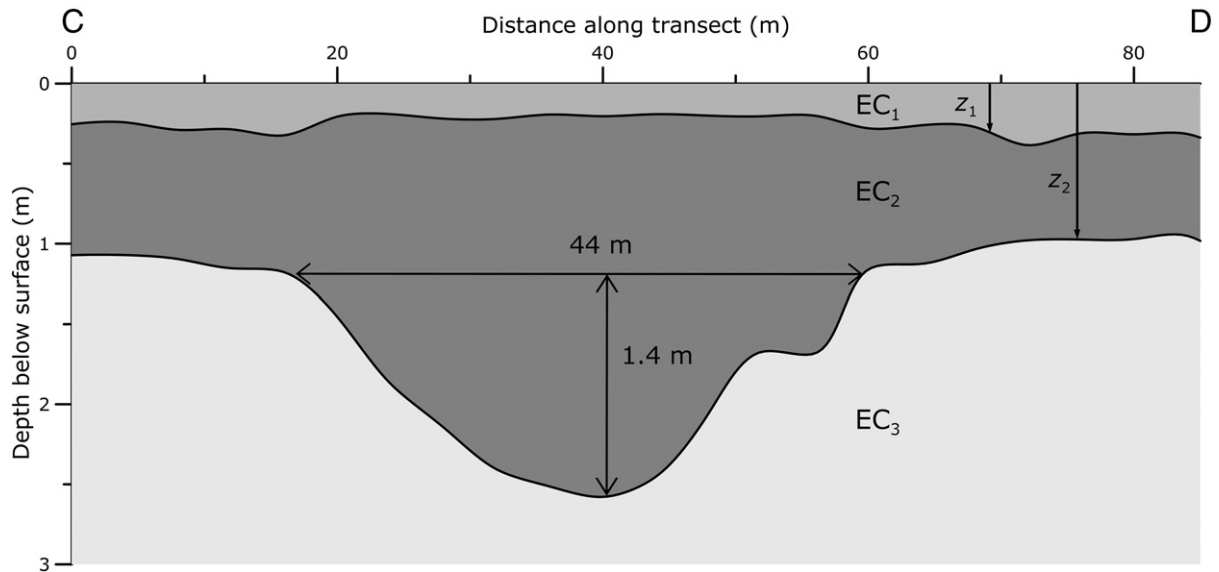


Fig. 7. Modelled build-up of the soil along transect CD, with indication of the width and maximal depth of the tidal channel.

Non-invasive, multi-receiver EMI sensors enable a more continuous mapping of the depths between contrasting layers by generating a high sampling density in a mobile configuration. Inversion approaches were developed (1) to discern smooth conductivity changes with depth (Monteiro Santos et al., 2010) and (2) to model the interface depths between contrasting soil layers in a two-layered soil (Saey et al., 2009a). While the first inversion technique can produce relatively high misfits in cases where sharp conductivity contrasts are present, the second method can in this case provide a more precise estimation of the interfaces depths, although a simplified soil model was needed (De Smedt et al., 2011).

The applicability of the method developed in this study situates in the ability to map more than one 'sharp' interface between contrasting soil layers continuously across the field by integrating multiple simultaneous signals from a multi-receiver EMI instrument. Because two different interfaces imply a three-layered soil model (with five unknown parameters), this soil model must be simplified by assuming the conductivity of one or two soil layers fixed across the study site. By performing a minimal amount of calibration observations, the values of these (approximately constant) conductivities can be estimated as their average values across the entire study site. This method is therefore generally applicable for three-layered soil profiles which consist of one or two layers with constant conductivities. Moreover, multi-receiver EMI instruments with more than 4 coil configurations enlarge the possibilities and potential to perform depth sounding without (or with limited amount of) the need for calibration observations.

## 10. Conclusions

The presented methodology allowed a precise prediction of the depth of the interfaces between the contrasting layers in a three-layered soil based on one survey with a multi-receiver EMI proximal sensor. However, the homogeneity and the conductivities of different soil horizons had to be determined from a limited number of borehole EC-measurements and soil augerings. This procedure offers a rapid and effective way to reveal micro-scale variations in depth of both interfaces between three contrasting soil layers three-dimensionally. In the coastal area, the detailed quantification of the horizontal and vertical extent of an ancient tidal channel allows to formulate answers to archaeological questions about the medieval landscape.

## Acknowledgements

This research was funded by the Municipality of Koksijde. The authors would like to thank Valentijn Van Parys and Hans Vermeersch for their assistance with the field work.

## References

- Baeteman, C., 1991. Chronology of coastal plain development during the Holocene in West Belgium. *Quaternaire* 2, 116–125.
- Baeteman, C., 1999. The Holocene depositional history of the IJzer palaeovalley (Western Belgian coastal plain) with reference to the factors controlling the formation of intercalated peat beds. *Geologica Belgica* 2, 39–72.
- Baeteman, C., 2008. Radiocarbon-dated sediment sequences from the Belgian coastal plain: testing the hypothesis of fluctuating or smooth late-Holocene relative sea-level rise. *The Holocene* 18, 1219–1228.
- Baeteman, C., Declercq, P.-Y., 2002. A synthesis of early and middle Holocene coastal changes in the western Belgian lowlands. *Belgeo* 2, 77–107.
- Bertrand, S., Baeteman, C., 2005. Sequence mapping of Holocene coastal lowlands: the application of the Streif classification system in the Belgian coastal plain. *Quaternary International* 133–134, 151–158.
- Brenning, A., Koszinski, S., Sommer, M., 2008. Geostatistical homogenization of soil conductivity across field boundaries. *Geoderma* 143, 254–260.
- Cockx, L., Van Meirvenne, M., De Vos, B., 2007. Using the EM38DD soil sensor to delineate clay lenses in a sandy forest soil. *Soil Science Society of America Journal* 71, 1314–1322.
- Corwin, D.L., Lesch, S.M., Oster, J.D., Kaffka, S.R., 2006. Monitoring management-induced spatio-temporal changes in soil quality through soil sampling directed by apparent electrical conductivity. *Geoderma* 131, 369–387.
- Coulouma, G., Samyn, K., Grandjean, G., Follain, S., Lagacherie, P., 2012. Combining seismic and electric methods for predicting bedrock depth along a Mediterranean soil toposequence. *Geoderma* 170, 39–47.
- De Smedt, P., Van Meirvenne, M., Meerschman, E., Saey, T., Bats, M., Court-Picon, M., De Reu, J., Werbrouck, I., Zwertvaegher, A., Antrop, M., Bourgeois, J., De Maeyer, P., Finke, P.A., Verniers, J., Crombé, P., 2011. Reconstructing palaeochannel morphology with a mobile multi-coil electromagnetic induction sensor. *Geomorphology* 130, 136–141.
- Domsch, H., Giebel, A., 2004. Estimation of soil textural features from soil electrical conductivity recorded using the EM38. *Precision Agriculture* 5, 389–409.
- Ervynck, A., Baeteman, C., Demiddelde, H., Hollevoet, Y., Pieters, M., Schelvis, J., Tys, D., Van Strydonck, M., Verhaege, F., 1999. Human occupation because of a regression, or the cause of a transgression? A critical review of the interaction between geological events and human occupation in the Belgian coastal plain during the first millennium AD. *Probleme der Küstenforschung im südlichen Nordseegebiet* 26, 97–121.
- Goovaerts, P., 1997. *Geostatistics for Natural Resources Evaluation*. Oxford University Press, New York.
- Kværnø, S.H., Haugen, L.E., Børresen, T., 2007. Variability in topsoil texture and carbon content within soil map units and its implications in predicting soil water content for optimum workability. *Soil and Tillage Research* 95, 332–347.
- Lück, E., Rühlmann, J., 2008. Electrical conductivity mapping with *Geophylus electricus*. Near Surface 2008, the 14th European Meeting of Environmental and Engineering Geophysics, Kraków, Poland, 15–17th of September 2008.

- Marquardt, D., 1963. An algorithm for least-squares estimation of nonlinear parameters. *SIAM Journal on Applied Mathematics* 11, 431–441.
- Massuel, S., Favreau, G., Desclotres, M., Le Troquer, Y., Albouy, Y., Cappelaere, B., 2011. Deep infiltration through a sandy alluvial fan in semiarid Niger inferred from electrical conductivity survey, vadose zone chemistry and hydrological modeling. *Catena* 67, 105–118.
- McBratney, A., Minasny, B., Whelan, B.M., 2005. Obtaining 'useful' high-resolution soil data from proximally-sensed electrical conductivity/resistivity (PSEC/R) surveys. In: Stafford, J.V. (Ed.), *Precision agriculture '05*. Wageningen Academic Publishers, Wageningen, pp. 503–510.
- McNeill, J.D., 1980. Electromagnetic terrain conductivity measurement at low induction numbers. Technical Note TN-6. Geonics Limited, Missisauga, Ontario, Canada.
- Monteiro Santos, F.A., Triantafyllis, J., Bruzgulis, K.E., Roe, J.A.E., 2010. Inversion of multiconfiguration electromagnetic (DUALEM-421) profiling data using a one-dimensional laterally constrained algorithm. *Vadose Zone Journal* 9, 117–125.
- Rhoades, J.D., Van Schilfgaarde, J., 1976. An electrical conductivity probe for determining soil salinity. *Soil Science Society of America Journal* 40, 647–651.
- Saey, T., Simpson, D., Vitharana, U., Vermeersch, H., Vermang, J., Van Meirvenne, M., 2008. Reconstructing the paleotopography beneath the loess cover with the aid of an electromagnetic induction sensor. *Catena* 74, 58–64.
- Saey, T., Simpson, D., Vermeersch, H., Cockx, L., Van Meirvenne, M., 2009a. Comparing the EM38DD and DUALEM-21S Sensors for Depth-to-Clay Mapping. *Soil Science Society of America Journal* 73, 7–12.
- Saey, T., Van Meirvenne, M., Vermeersch, H., Ameloot, N., Cockx, L., 2009b. A pedotransfer function to evaluate the soil profile textural heterogeneity using proximally sensed apparent electrical conductivity. *Geoderma* 150, 389–395.
- Saey, T., Van Meirvenne, M., Dewilde, M., Wyffels, F., De Smedt, P., Meerschman, E., Islam, M.M., Meeuws, F., Cockx, L., 2011. Combining multiple signals of an electromagnetic induction sensor to prospect land for metal objects. *Near Surface Geophysics* 9, 309–317.
- Samouëlian, A., Cousin, I., Tabbagh, A., Bruand, A., Richard, G., 2005. Electrical resistivity survey in soil science: a review. *Soil and Tillage Research* 83, 173–193.
- Smirnov, A., Paradis, S.J., Boivin, R., 2008. Generalizing surficial geological maps for scale change: ArcGis tools vs. cellular automata model. *Computers & Geosciences* 34, 1550–1568.
- Sudduth, K.A., Drummond, S., Kitchen, N.R., 2001. Accuracy issues in electromagnetic induction sensing of soil electrical conductivity for precision agriculture. *Computers and Electronics in Agriculture* 31, 239–264.
- Sudduth, K.A., Kitchen, N.R., Wiebold, W.J., Batchelor, W.D., Bollero, G.A., Bullock, D.G., Clay, D.E., Palm, H.L., Pierce, F.J., Schuler, R.T., Thelen, K.D., 2005. Relating apparent electrical conductivity to soil properties across the north-central USA. *Computers and Electronics in Agriculture* 46, 263–283.
- Triantafyllis, J., Odeh, I.O.A., McBratney, A.B., 2001. Five geostatistical models to predict soil Salinity from electromagnetic induction data across irrigated cotton. *Soil Science Society of America Journal* 65, 869–878.
- Vitharana, U.W.A., Saey, T., Cockx, L., Simpson, D., Vermeersch, H., Van Meirvenne, M., 2008. Upgrading a 1/20,000 soil map with an apparent electrical conductivity survey. *Geoderma* 148, 107–112.
- Wait, J.R., 1962. A note on the electromagnetic response of a stratified earth. *Geophysics* 27, 382–385.
- Webster, R., Oliver, M.A., 2007. *Geostatistics for Environmental Scientists*, Second Edition. John Wiley & Sons, Chichester.
- Wilson, R.C., Freeland, R.S., Wilkerson, J.B., Hart, W.E., 2005. Interpolation and data collection error sources for electromagnetic induction-soil electrical conductivity mapping. *Applied Engineering in Agriculture* 21, 277–283.